The Crucial Importance of Chemistry in the Structure−Function Link: Manipulating Hydrogen Bonding in Iron-Containing Superoxide Dismutase[†,‡]

Emine Yikilmaz,[§,||,⊥] David W. Rodgers,*[,#] and Anne-Frances Miller*[,§,||,#]

Department of Chemistry, University of Kentucky, Lexington, Kentucky 40506, Department of Chemistry, The Johns Hopkins University, Baltimore, Maryland 20208, and Department of Molecular and Cellular Biochemistry and Center for Structural Biology, University of Kentucky Medical Center, Lexington, Kentucky 40536

Received July 27, 2005; Revised Manuscript Received November 11, 2005

ABSTRACT: Fe-containing superoxide dismutase's active site Fe is coordinated by a solvent molecule, whose protonation state is coupled to the Fe oxidation state. Thus, we have proposed that H-bonding between glutamine 69 and this solvent molecule can strongly influence the redox activity of the Fe in superoxide dismutase (SOD). We show here that mutation of this Gln to His subtly alters the active site structure but preserves 30% activity. In contrast, mutation to Glu otherwise preserves the active site structure but inactivates the enzyme. Thus, enzyme function correlates not with atom positions but with residue identity (chemistry), in this case. We observe strong destabilization of the Q69E-FeSOD oxidized state relative to the reduced state and intermediate destabilization of oxidized Q69H-FeSOD. Indeed, redox titrations indicate that mutation of Gln69 to His increases the reduction potential by 240 mV, whereas mutation to Glu appears to increase it by more than 660 mV. We find that this suffices to explain the mutants' loss of activity, although additional factors may also contribute. The strongly elevated reduction potential of Q69E-FeSOD may reflect reorganization of the active site H-bonding network, including possible reversal of the polarity of the key H-bond between residue 69 and coordinated solvent.

The quest to understand relationships between protein structure and function is one of the pervasive themes in structural biology. Relationships between sequence, structure, and function have now become important assumptions used to propose roles for newly discovered genes and proteins, and a tool in designing and modifying existing proteins. However evolution has proven a creative innovator, employing unrelated structures for the same function [witness the different families of peptidases or of superoxide dismutases (SODs)[1] (*2*)] and utilizing the same structure to support disparate functions [aconitase/iron-regulatory protein (*3*, *4*), enolase/phosphatase E1 (*5*), and TIM barrel proteins (*6*, *7*)]. This is particularly important in cases where the activity depends on aspects not rigorously interrogated by the structural method, which may therefore be inferred instead. Thus, where the protonation state of an amino acid, the identity of a metal ion, or the nature of hydrogen bonds (H-bonds) plays crucial roles in activity, it may not be possible to fully understand function from the quality of data normally sufficient to determine a protein's structure.

Redox-active enzymes, which comprise a substantial fraction of enzymes in general, constitute a case in point. Proton transfer is commonly associated with electron transfer, and H-bonds to ligands play important roles in tuning the reactivity of redox centers (*8*−*12*). Therefore, the locations of labile protons, the existence of H-bonds, and even their polarities become important ingredients in function. The possibilities of apprehending these and of manipulating them intentionally are thus exceedingly powerful tools in understanding and modifying enzyme activity. The following provides a striking example in which change of a single non-hydrogen atom, readily accommodated without obvious alteration of the three-dimensional structure, produces drastic changes in activity. These may be explained on the basis of altered H-bonding in the active site, instead.

The structure and mechanism of FeSOD from *Escherichia coli* are relatively well understood (*13*−*19*). The enzyme is isolated as a dimer of 22 kDa monomers, each containing an independent active site. The active site contains a single Fe ion coordinated in roughly trigonal bipyramidal geometry by two His and an Asp^- as equatorial ligands and a third His and a molecule of solvent as axial ligands (Figure 1, top). The coordinated solvent engages in an H-bond with the Asp^- ligand and another with the conserved active site Gln69.[2]

[†] A.-F.M. is pleased to thank the NSF for financial support (Grant MCB 0129599).

[‡] Coordinates and structure files have been deposited and will be released upon publication of this work: PDB codes 2BKB and 1ZA5.

* Address correspondence to these authors. A.-F.M.: e-mail, afm@uky.edu; tel, (859) 257-9349; fax, (859) 323-1069. D.W.R.: e-mail, rodgers@focus.gws.uky.edu; tel, (859) 257-5205; fax, (859) 323-1037.

[§] University of Kentucky.

[||] The Johns Hopkins University.

[⊥] Current address: Berlex Biosciences, 2600 Hilltop Drive, Systems Biology, Richmond, CA 94806.

[#] University of Kentucky Medical Center.

[1] Abbreviations: E_m, the reduction potential (the excess stability of the reduced state over the oxidized state); EPR, electron paramagnetic resonance; IPTG, isopropyl β-D-thiogalactopyranoside; PEG, poly(ethylene glycol); PIPES, piperazine-*N*,*N*′-bis(2-ethanesulfonic acid); rmsd, root mean square deviation; SOD, superoxide dismutase; Tris, tris(hydroxymethyl)aminomethane; WT, wild type, not mutated.

[2] Numbering of *E. coli* FeSOD and MnSOD is used throughout.

10.1021/bi051495d CCC: $33.50
Published on Web 01/07/2006

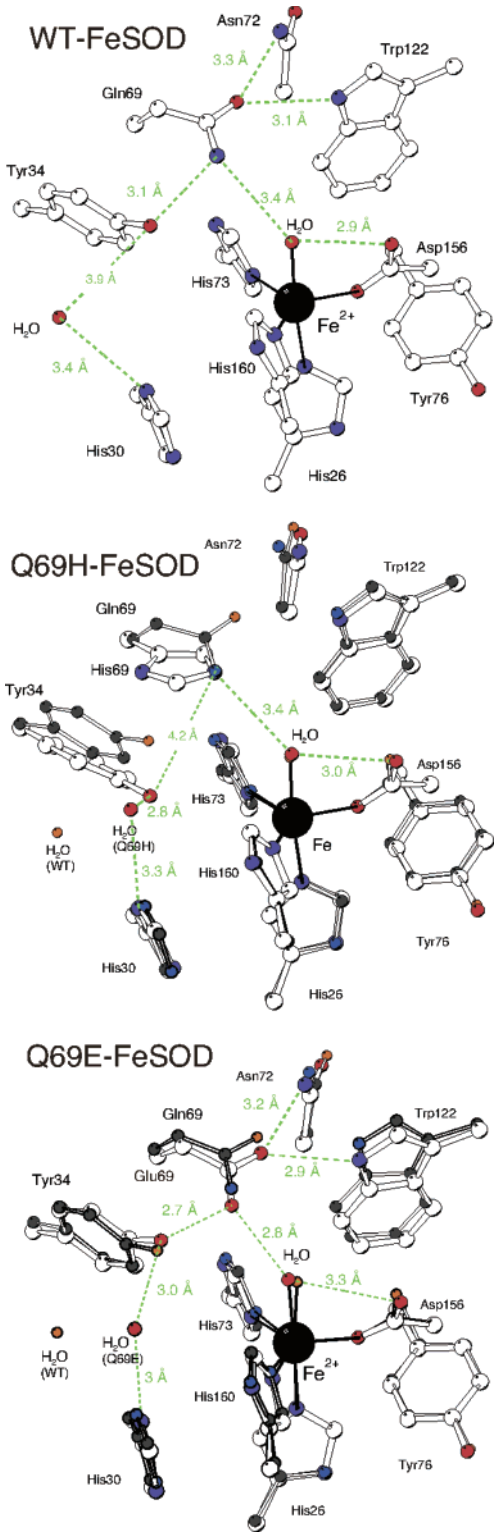

FIGURE 1: Active sites of wild-type (WT) Fe^{2+}SOD (top), Q69H-FeSOD overlain with WT (middle), and Q69E-Fe^{2+}SOD overlain with WT (bottom). H-bonds are shown as dotted lines. Top: WT distances and structure are based on 1ISA.pdb for WT-Fe^{2+}SOD (*13*). The separation between Tyr34 and channel H_2O is also indicated for comparison with the mutants. Middle: The structure of Q69H-FeSOD is shown with larger white C atoms and wider bonds, whereas WT-Fe^{3+}SOD is shown with C atoms in black and narrow bonds [based on coordinates of 1ISB.pdb (*13*)]. Q69H distances refer to the Q69H-FeSOD structure only. Bottom: The structure of Q69E-Fe^{2+}SOD is shown with larger white C atoms and wider bonds, whereas WT-Fe^{2+}SOD is shown with smaller C atoms in black [based on coordinates of 1ISA.pdb (*13*)]. Q69E distances refer to the Q69E-Fe^{2+}SOD structure only.

The catalytic Fe ion and coordinated solvent molecule are believed to cycle between $Fe^{3+}-OH^-$ and $Fe^{2+}-H_2O$ in the course of turnover [eq 1 (*15*, *20*)]:

$$O_2^{\bullet -} + H^+ + PFe^{3+}-OH^- \rightarrow O_2 + PFe^{2+}-OH_2 \quad (1a)$$

$$O_2^{\bullet -} + H^+ + PFe^{2+}-OH_2 \rightarrow H_2O_2 + PFe^{3+}-OH^- \quad (1b)$$

where P stands for the SOD protein. Uptake of an electron in (1a) is thus coupled to acquisition of a proton, and the proton released upon reoxidation of Fe is believed to contribute to product formation in (1b). From pH 7 to pH 10, the oxidation state of the Fe is coupled to the protonation state of coordinated solvent (*20*, *21*).

However, the protonation state of the coordinated solvent is itself expected to be strongly influenced by its H-bond with Gln69, which in turn H-bonds to Tyr34, Asn72, and Trp122 in a network that links it with other elements of secondary structure (Tyr34) and even the other domain of the protein (Trp122, Figure 1, top). Thus, interactions with the rest of the protein polarize the Gln and constrain it to unfavorable H-bond donation to coordinated H_2O in reduced FeSOD (*10*, *22*). Indeed, several mutations of the analogous Gln in MnSOD produce significantly higher than WT thermal stability (*23*, *24*), indicating that some of the interactions of this residue are costly to the protein overall. These and other mutations of the active site Gln also significantly alter the E_m (*10*, *22*, *25*, *26*), consistent with our proposal that the H-bond between Gln69 and coordinated solvent exerts an important influence on the relative stabilities of coordinated H_2O vs OH^- and, thereby, the E_m (*1*, *10*, *22*). Since proton transfer coupled to electron transfer is the norm in biological chemistry, we proposed that proteins' exquisite and strong control over the p*K*s and degrees of protonation of functionalities coupled to the redox sites, can provide a general and very important mechanism of redox tuning in enzymes (*27*, *57*).

Since we have proposed that the FeSOD protein employs H-bonds to tune Fe's reactivity, we now seek to intentionally manipulate H-bonds in the active site via the structurally conservative Gln to Glu substitution, or alternatively the chemically conservative Gln to His substitution, at position 69. His69, like Gln, has the possibility of either donating or accepting an H-bond. We find that Q69H-FeSOD retains an H-bond with coordinated solvent but that, in the absence of H-bonds to the rest of the network, it is no longer *constrained* to unfavorable H-bond *donation*, consistent with a significant increase in reduced state stability (and E_m). However, Q69E-FeSOD is fully reduced as isolated and has a strongly elevated E_m, consistent with Glu's ability to donate at most only one H-bond, vs Gln's ability to donate two. Although other factors may also contribute, the increases in E_m are sufficient to explain most of the activity loss, despite apparent retention of all residue positions (with replacement of Gln's N by Glu's O) in the Q69E mutant.

MATERIALS AND METHODS

Proteins. Genes encoding mutant versions of FeSOD were constructed from the gene for the WT by PCR using the megaprimer method (*28*). The SOD gene sequence was confirmed to contain only the desired mutation by restriction

analysis (*Aat*II, *Xho*I, *Xba*I) and sequencing of both DNA strands. The protein was overexpressed in cultures growing in LB or minimal medium supplemented with ampicillin, kanamycin (25 μg/mL each), and either 0.1 mM $FeCl_2$ or 25 μM $MnCl_2$, upon induction with 0.1−0.4 mM IPTG when the optical density at 600 nm reached 1. Cultures were harvested 4 h later, and the SOD protein was purified as described elsewhere (*17*, *29*). Protein concentrations were estimated on the basis of the extinction coefficient at 280 nm for WT-FeSOD of 10.1×10^4 M^{-1} cm^{-1} (*29*). Metal ion content was determined by atomic absorption spectroscopy, and specific activity was measured on the basis of SOD's interference with reduction of cytochrome *c* by superoxide (*30*).

Crystal Structure Determination. Crystals were grown by the hanging drop method. Platelike crystals were obtained from 5 μL of 6.5 mg/mL Q69H-FeSOD protein (in 10 mM PIPES, pH 7.4) diluted 1:1 in 1050 mM $MgCl_2$, 16% (w/v) PEG 8000, and 20 mM Tris-HCl at pH 8.66. Crystals reached their final size in 3−7 days at 4 °C. Crystals were soaked in a cryoprotection medium of 840 mM $MgCl_2$, 16 mM Tris-HCl (pH 8.00), 20% (w/v) PEG 8000, and 20% (v/v) ethylene glycol, mounted in a nylon loop, and then flash-cooled in liquid N_2 (*31*). Diffraction data were collected using 1.5418 Å Cu Kα radiation from a Rigaku RU200 rotating anode generator and collected on an R-axis IV detector 150 mm from the crystal; 180° of data were collected with 1° oscillations and 30 min per frame. The crystals diffracted to 1.8 Å.

Rhombic crystals of Q69E-Fe^{2+}SOD were obtained from a 1:1 dilution of 13.7 mg/mL protein in 10 mM PIPES (pH 7.4) with a crystallization buffer of 100 mM ammonium acetate (pH 5.7), 10 mM sodium citrate, and 22.5% PEG 4000. Diffraction data were collected as above but with the detector 110 cm from the crystal. The crystals diffracted to 1.5 Å.

X-ray diffraction peaks were integrated using HKL (*32*). Peak intensities were converted to amplitudes and scaled using CCP4 (Collaborative Computational Project, 1994). Initial phases were obtained by molecular replacement using the structure of WT-Fe^{3+}SOD as the model [1ISB.pdb (*13*)], using CNS (*33*). For Q69H-FeSOD, a translation/rotation search (15−4 Å data), followed by one cycle of rigid-body refinement using data corresponding to 20−1.8 Å resolution gave a single solution and $R = 35.25\%$ ($R_{free} = 35.29\%$). The structure of Q69H-FeSOD was used as the model for Q69E-FeSOD. Molecular replacement (20−4 Å data) and rigid-body refinement over 20−1.6 Å data yielded a single solution with $R = 36.21\%$ ($R_{free} = 36.16\%$). Simulated annealing was performed in 1000 steps as the system was cooled from a simulated temperature of 2500 K. Additional 100 step refinement at 300 K produced an *R*-factor of 28.96% ($R_{free} = 31.94\%$) for Q69H-FeSOD and 30.85% ($R_{free} = 32.64\%$) for Q69E-FeSOD. The molecular graphics package O was used for inspection and rebuilding of the structure (*34*). Residue 69 was listed as Ala in the amino acid sequence used to fit the data, and the occupancies of the active site Fe and its coordinated solvent were also set to zero, to permit visualization of difference electron density corresponding to the His69 (or Glu69) side chain, Fe, and coordinated solvent.

Table 1: Summary of Crystallographic Parameters, Results, and Figures of Merit

	Q69H-FeSOD	Q69E-FeSOD
Data Collection Statistics		
space group	$P2_1$	$P2_1$
unit cell *a*, *b*, *c* (Å)	41.2, 84.9, 61.6	43.5, 107.7, 84.2
β (deg)	108.37	95.02
molecule in asymmetric unit	one dimer	two dimers
solvent content (%) ($d = 1.3$ g/mL)	47.57	45.04
wavelength (Å)	1.5418	1.5418
temperature (K)	115	115
resolution limit (Å)	1.8	1.7
last shell (Å)	1.88−1.80	1.76−1.70
unique reflections	32864	79209
average redundancy (last shell)	3.1 (1.6)	1.8 (1.8)
R_{merge} (last shell)[a]	0.06 (0.23)	0.06 (0.13)
$I/\sigma I$ (last shell)	16.9 (3.0)	13.4 (5.8)
completeness (%)	88	93.4
Refinement		
R_{work}/R_{free}[b,c]	0.20/0.24	0.20/0.23
no. of residues (protein/Fe/water/Tris)	384/2/459/4	768/4/629/0
av *B* (main chain/ side chain, Å^2)	25/26	13/14
B rmsd bonded main chain	1.0	1.0
B rmsd bonded side chain	1.7	1.8
rmsd bond lengths (Å)	0.005	0.005
rmsd bond angles (deg)	1.7	1.2
rmsd improper angles (deg)	1.3	0.8
rmsd dihedral angles (deg)	21.2	21.2
Ramachandran plot		
core (%)	90.2	91.1
allowed (%)	8.0	7.1
generously allowed (%)	1.2	1.2
disallowed (%)	0.6	0.6
Luzzati coordinate error (Å)	0.23	0.19
Luzzati cross-validated error (Å)	0.28	0.22
PDB entry	1ZA5	2BKB

[a] $R_{merge} = \sum\sum_i |I_i - \langle I \rangle| / \sum_i I_i$, with the sum taken over all unique reflections; $\langle I \rangle$ is the mean intensity. [b] $R_{work} = (\sum |F_o| - |F_c| / \sum F_o)$, based on 90% of the reflections that were used in refinement. [c] R_{free} was calculated as for R_{work} but based on 10% of the reflections that were not used as the basis for the refinement.

Water molecules were added on the basis of data from 20 to 1.8 Å (1.6 Å for Q69E), where $|F_o - F_c|$ electron density peaks exceeded 3σ and the putative waters were well positioned to hydrogen bond with plausible partners. Energy minimization and then refinement of atomic *B*-factors followed by a second round of water picking and refinement produced a final Q69H-FeSOD model including 384 amino acid residues, two Fe(III) ions and two coordinated water molecules, 459 water molecules, and 4 molecules of Tris identified on the surface of the protein, with an *R*-factor of 20.17% ($R_{free} = 23.90\%$, Table 1) (Supporting Information, Figure 2). A similar refinement sequence was used for Q69E-FeSOD, arriving at final *R*-factors of $R = 20.74$ and $R_{free} = 23.14$.

Redox Titrations and Determination of Limiting Values. Redox titrations were performed at 10 °C in a degassed airtight cell fitted with an Ag/AgCl and Pt combination electrode (Microelectrodes Inc.). The redox titrant was 170 mM dithionite in degassed 100 mM KOH, and the combination electrode was calibrated with quinhydrone at two pH values ($E_m = 263$ and 86 mV at pH = 4 and 7, respectively,

Table 2: Biochemical Comparison of WT and Mutant SODs Studied

SOD type	Fe content (% active sites)	Mn content (% active sites)	specific activity (units/mg of protein)	Fe oxidation state (as-isolated)	Mn oxidation state (as-isolated)
WT-FeSOD	90	none detectable	6070	3+	−
Q69H-FeSOD	55	32	1030	2+/3+	2+
Mn-substituted Q69H-FeSOD	10	90	300	2+/3+	2+
Q69E-FeSOD	>95	none detectable	3	2+	−
WT-MnSOD	3−5	>90	6000	−	2+/3+

at 25 °C). All potentials are quoted vs the normal hydrogen electrode (NHE).

Ten milliliters of 0.86 mM WT-FeSOD dimers in a buffer of 100 mM KBr, 100 mM PIPES, pH 7.4, and 10% glycerol was supplemented with a cocktail of redox mediators at the following final concentrations: 38.72 μM 2,2-dichloroindophenol ($E° = 217$ mV), 44.80 μM toluylene blue ($E° = 115$ mV), 59.83 μM thionine ($E° = 64$ mV), 47.59 μM methylene blue ($E° = 11$ mV), 49.60 μM indigo trisulfonate ($E° = -81$ mV), and 44.60 μM indigo carmine ($E° = -125$ mV). The sample was degassed and then allowed to equilibrate overnight (10−12 h) before the first measurement. Reductant was added in 2−4 μL aliquots, and the system was evacuated and refilled with Ar after each addition. The optical spectrum and the electrode reading were used to monitor the system's approach to equilibrium, which was achieved within 2 h of each addition of titrant. The reduction potential was then recorded, and 250 μL of solution was transferred anaerobically to an Ar-filled septum-sealed 4 mm EPR tube and frozen immediately by immersion in liquid N_2. EPR derivative amplitude at $g' = 4.8$, corresponding to oxidized active sites ([ox]), was plotted as a function of measured reduction potential (E), and the curve was fit with the Nernst equation (eq 2).

$$[\mathrm{ox}] = [\mathrm{ox}_{\mathrm{max}}]/(1 + e^{-(nF/RT)(E-E_m)}) \quad (2)$$

The E_m of Q69H-FeSOD was determined by the same method, but the mediators present and their final concentrations were 47.99 μM ferrocene ($E° = 422$ mV), 193.11 μM potassium ferricyanide ($E° = 360$ mV), 58.39 μM 1,1′-dimethylferrocene ($E° = 341$ mV), 51.71 μM 2,2-dichloroindophenol ($E° = 217$ mV), and 47.59 μM toluylene blue ($E° = 115$ mV), as required by the different reduction potential of this FeSOD.

Limits on the E_m of Q69E-FeSOD were obtained by determining what oxidants were able to oxidize it. All oxidants were first assayed for ability to oxidize WT-Fe^{2+}SOD (generated by reduction of degassed WT-Fe^{3+}SOD with dithionite). $KMnO_4$, K_2IrCl_6, $K_3Fe(CN)_6$, and $NaIO_4$ were prepared as ≈2 mM aqueous solutions and added to WT- or Q69E-Fe^{2+}SOD. KO_2 was dissolved in DMSO with the aid of the crown ether 18-crown-6 (*15*). 2,4-Naphthoquinone sulfonate was added to FeSOD either as a degassed solution or by addition of a small amount of the solid, followed by gentle mixing to dissolve it. Oxidant-treated FeSOD samples were frozen in EPR tubes once all visible changes had ceased or after overnight incubation at 4 °C if no visible changes were evident. EPR spectroscopy was used to observe any oxidized Fe^{3+}SOD sites generated upon treatment with oxidant.

EPR spectra were collected at 110 K on a Bruker EMX 300 operating at X band (9.47 GHz) at a nominal power of 20 mW using 10 G modulation at 100 kHz.

RESULTS

Description of the Proteins. The Q69E and Q69H mutants of FeSOD were overexpressed at levels comparable to WT, although Q69H-FeSOD proved to have somewhat weaker Fe ion binding affinity and specificity (Table 2). Nonetheless, Q69H-FeSOD retained significant activity, consistent with the chemically conservative nature of the substitution, and the precedent in extremophyllic FeSODs for a His in the position of the active site Gln (*35*−*38*). In a comparison of preparations with varying Fe and Mn incorporation, specific activity correlated with Fe content. Therefore, activity appears to stem primarily from Fe-containing sites. When the specific activity observed is corrected for incomplete Fe incorporation, it corresponds to approximately 30% of WT-FeSOD's specific activity (i.e., on a per Fe basis). In contrast, Q69E-FeSOD binds Fe selectively and quantitatively but is inactive in the standard assay.

The two SOD mutants are also significantly different with respect to the oxidation state of the metal ion stabilized. Although WT-FeSOD was isolated fully oxidized (Fe^{3+}) on the basis of the absence of NMR resonances characteristic of the reduced state, Q69H-FeSOD was ≈30% reduced, and Q69E-FeSOD remained fully reduced (all Fe as Fe^{2+}). Thus, it appears that the E_m of Q69H-FeSOD is higher than WT's, and Q69E-FeSOD's is much higher still.

Results of Crystallography: Fold and General Features. Both mutant SODs crystallized readily, although Q69E-FeSOD's unit cell was larger and contained four monomers, whereas Q69H-FeSOD's unit cell contained a single dimer, as for the WT (Supporting Information, Figure 1). The backbone folds of Q69H- and Q69E-FeSOD were essentially the same as that of the WT-FeSOD, with rmsds from WT of 1.24 and 0.72 Å, respectively, based on superposition of the Cα atoms of dimers (Figure 2). Larger deviations were concentrated in external loops and residues with higher *B*-factors.

Thus, one observes the WT architecture consisting of two domains, with the smaller N-terminal domain dominated by three α helices and the C-terminal domain comprising a three-stranded β sheet largely shielded from solvent by four α helices on the convex face. The concave face is largely protected from solvent by its packing with the N-terminal domain (Supporting Information, Figure 2). Three residues lie outside the most favored region of the Ramachandran plot: Ala84/284, Asn40/340, and Arg167/367 have outlier ϕ/ψ values imposed upon them by the local backbone arrangement. As in the WT protein, there is a kink in the first α helix near residue 28 (Supporting Information, Figure 2), with backbone *B*-factors slightly *lower* than the average *B*-factor, for both mutants. This feature is likely important to function, as it is seen in many crystal structures of FeSOD and MnSOD (*13*), and it affects the relative orientations of

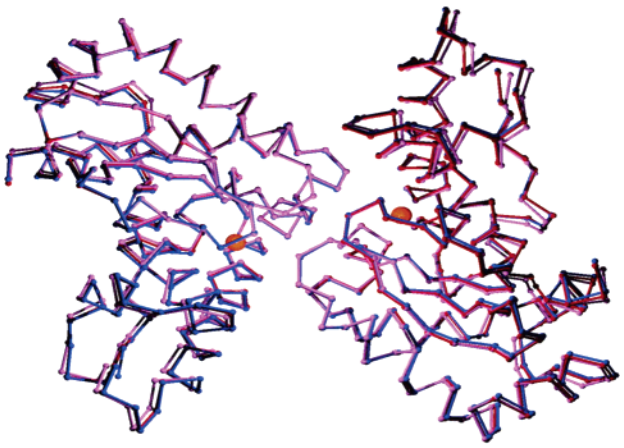

FIGURE 2: Overlay of the Cα traces of the dimers of Q69H-FeSOD (magenta), Q69E-FeSOD (red), and WT-FeSOD (blue), based on all 1536 backbone atoms of each protein, using the WT-FeSOD coordinates of 1ISB.pdb (*13*).

the ligand His26 and Tyr34 and His30, which flank the channel through which substrate is believed to access the active site (*13*). Moreover, Tyr34 is responsible for the reduced state active site p*K* near 8.5 and exerts important control over substrate specificity (*17*, *19*, *39*−*41*). In both mutants, Fe coordination geometry almost identical to that of the WT-FeSOD is retained (below).

In Q69H-FeSOD, the Fe B-factors of 18.2 and 19.3 Å^2 compare well with the overall average *B*-factor of 25 Å^2. The Fe and its ligands are better defined than the protein overall, whereas the second sphere residues Tyr34 and His69 are more similar to the rest of the protein with respect to *B*-factors (Table 3).

Q69E-FeSOD's *B*-factors are significantly lower (Table 3), as anticipated from the more homogeneous material and higher resolution limit of the data. The Fe's *B*-factors of 8.60, 8.73, 10.41, and 11.04 Å^2 are well below the overall average of 14 Å^2, as are the *B*-factors associated with the ligands. The second sphere residues 34 and 69 have *B*-factors more closely resembling those of the ligands and, therefore, appear more tightly coupled to the active site than to the rest of the protein (as in WT-FeSOD).

Active Site of Q69H-FeSOD. The active site of Q69H-FeSOD is very similar to that of the WT (Figure 1, middle) and deviates by an rmsd[3] of only 0.5 Å for unmutated side chain atoms. However, the orientation of the His69 ring differs from that of the parent Gln69 amide such that it does not come close enough to Trp122 and Asn72 to engage in H-bonds with them, whereas the WT- Gln69 does (Table 4). Similarly, His69 is imperfectly stacked with Tyr34 (Figure 3), and the distances between Tyr34's phenolic O and His69's three potential H-bonding positions are all 3.5 Å or greater. Thus, the slight extra bulk of His69, in addition to its shorter methylene linkage to the backbone, does not allow His to simultaneously H-bond with coordinated solvent, Tyr34, Asn72, and Trp122. Asn72 and Trp122 are buttressed by other residues and are not free to accommodate His69. Instead, His69 is displaced toward Tyr34, which is able to recede into the substrate access channel to accommodate His69. Indeed, Tyr34 is the unmutated residue with the largest displacement from the WT (rmsd = 1.2 Å for the side chain atoms). Loss of the WT H-bonds to Tyr34, Asn72, and Trp122 can account for His69's relatively high *B*-factor, compared to those of Gln69 and Glu69 in WT- and Q69E-FeSOD, respectively (Table 3).

Our electron density data are quite clear at 2σ that the His disposition and χ_1 used in Figure 3 are the best single fit to the density. Indeed, the *B*-factors for His69 are no higher than those for the rest of the protein (Table 3). However, in the absence of an H-bond with Trp122, the position nearest Trp122 could be either Cδ2 or Nδ1, presenting either the Nϵ2 or the Cϵ1 position, respectively, to coordinated solvent. We favor the former, because Nϵ2 is normally considered to be better at H-bonding and because of the slightly higher electron densities associated with the left-hand side δ and right side ϵ positions in Figure 3, which are therefore expected to correspond to the (more electronegative) N positions in the His ring. This latter observation should be regarded as tentative only, at our resolution of 1.8 Å. However, a weak H-bond with coordinated solvent appears to be retained (3.4 Å), as in WT. NMR and EPR spectroscopic titrations indicate that His69 is neutral (*9*), and neutral His is normally protonated on the Nϵ2. However, the preference is slight and our structure leaves open both possibilities: that His69 acts as an H-bond acceptor from coordinated H_2O or as an H-bond donor to coordinated solvent.

Another potential source of heterogeneity in the Q69H active site is the metal ion content. The preparation from which crystals grew contained Fe and Mn in a ratio of approximately 2:1, which accounted for just under 90% of the sites. All Mn was reduced, based on EPR and optical spectrophotometry. However, Fe was partially reduced. Since the parameters ascribed by CNS to Fe(II), Fe(III), and Mn(II) are very similar (other than charge), our 1.8 Å resolution does not distinguish between these ions, and the structural model obtained reflects averaged properties of the different types of sites. Thus, special attention was devoted to the metal center in the course of refinement. In early rounds of refinement we set the metal ion occupancy to 1.0 and the metal ion identity to Fe(III). Subsequent refinement trials with a large range of different starting occupancies and *B*-factors yielded an occupancy between 0.9 and 1.1 and a *B*-factor between 16 and 20 Å^2. Thus, the structure represents predominantly metalated sites, and the *B*-factor associated with the metal ion is close to those obtained for the rest of the active site residues (Table 3). We conclude that the active site metal ion is not an important source of uncertainty.

During all refinements, density corresponding to the coordinated solvent molecule was clearly evident adjacent to the metal ion and was allowed to refine freely as a water molecule. As for WT and Q69E, the distance between Fe and the Asp$^-$ ligand O is shorter than the other coordination distances in Q69H-FeSOD. However, in contrast to WT and Q69E, the Fe-to-O distance for coordinated solvent is longer than the average coordination distance in Q69H-FeSOD. Thus, mutation of Gln69 to His appears to have made coordinated solvent a weaker ligand. This cannot be simply a result of the partial reduction of the site, as even the reduced state structure of the WT FeSOD displays an Fe-to-O distance for coordinated solvent that is shorter than the distances to the His ligand N's (Table 4).

[3] Calculated for an active site overlay based on residues 26, 30, 34, 73, 76, 122, 156, 158, 160, and 161.

Table 3: Comparison of *B*-Factors Obtained for Different FeSOD Structures (Å^2)[a]

protein	all protein atoms	backbone	side chains	Fe	coordinated solvent	amino acid ligands	residue 69	residue 34
Q69H	25 (6)	25 (5)	26 (7)	18.7 (0.6)	15.4 (0.9)	18 (2)	25 (4)	22 (3)
Q69E	14 (6)	13 (4)	14 (6)	10 (1)	9 (2)	8 (2)	9 (2)	11 (2)
WT[b]	12 (8)	11 (6)	13 (9)	5.4 (0.2)	6 (3)	4 (1)	4.4 (0.8)	7 (2)

[a] Averages are given with standard deviation in parentheses; atoms were all assigned occupancies of 1.0. [b] FeSOD values are based on the coordinates 1ISB.pdb from Lah et al. (*13*). The resolution of this crystal structure is given as 1.85 Å with an R^2 of 18.4% [for the oxidized state, 1ISA.pdb, the resolution is given as 1.8 Å with $R^2 = 18.8\%$ (*13*)].

Table 4: Crystallographic Distances between Interacting Amino Acid Side Chains

	FeSOD type distances (Å)			
	Q69H	Q69E	Fe^{3+}SOD 1ISB.pdb	Fe^{2+}SOD 1ISA.pdb
ligands				
Fe−OD2 (Asp)	2.0 (0.04)	2.0 (0.01)	1.9 (0.02)	1.9 (0.02)
Fe−N (His26)	2.2 (0.01)	2.2 (0.04)	2.1 (0.01)	2.2 (0.01)
Fe−N (His73)	2.1 (0.02)	2.2 (0.05)	2.1 (0.02)	2.0 (0.02)
Fe−N (His160)	2.1 (0.05)	2.1 (0.05)	2.1 (0.01)	2.1 (0.01)
Fe−O (coord solvent)	2.2 (0.03)	2.1 (0.04)	2.0 (0.04)	2.0 (0.02)
coordinated solvent				
O−OD1 (Asp156)	3.0 (0.08)	3.3 (0.03)	3.0 (0.07)	2.9 (0.09)
O−NE2 (His69)	3.4 (0.01)			
or O−OD (Glu69)		2.8 (0.06)		
or O−ND (Gln69)			3.4 (0.08)	3.4
residue 69				
O (Tyr34)−NE2 (His69)	4.2 (0.1)			
or O−OD (Glu69)		2.7 (0.06)		
or O−ND (Gln69)			3.1 (0.04)	3.1
O (Asn72)−NE2 (His69)	4.3 (0.1)			
or N (Asn72)−O (Gln69 or Glu69)		3.2 (0.05)	3.4	3.3 (0.04)
N (Trp122)−NE2 (His69)	3.9 (0.2)			
or N (Trp122)−O (Gln69 or Glu69)		2.9 (0.06)	3.1 (0.03)	3.1 (0.03)
channel solvent				
O−O (Tyr34)	2.8 (0.3)	3.0 (0.2)	3.7 (0.2)	3.9 (0.02)
O−ND1 (His30)	3.3 (0.03)	3 (1)	3.5 (0.1)	3.4 (0.03)
O−Fe	6.5 (0.03)	6.3 (0.8)	7.0 (0.5)	7.6 (0.2)
His73−Fe−His160 angle (deg)	127.4 (0.6)	127 (2)	127.9 (0.5)	126.6 (0.4)

Q69E-FeSOD. Q69E-FeSOD was refined with the active site Fe assigned to Fe^{2+} at full occupancy of 1.0, in accordance with our spectroscopic and analytical results. The active site of Q69E-Fe^{2+}SOD is essentially superimposable on that of WT-Fe^{2+}SOD (Figure 1, bottom). The Glu69 side chain appears to make a very good H-bond with coordinated solvent, based on an O−O distance of 2.81 (0.06) Å (Table 4). Glu69 also retains the other three H-bonds, with Asn72, Trp122, and Tyr34, that characterize Gln69 in the WT active site. The atoms[4] of Glu69 display an rmsd of 0.5 Å from those of WT's Gln69, with which it is close to superimposable, although Glu69 is significantly closer to coordinated solvent than either His69 or Gln69 (Table 4). The other active site amino acid that appears slightly displaced by this mutation is Tyr34, with an rmsd from WT of 0.3 Å (also slightly lower than the 0.7 Å backbone rmsd between the two structures). The good H-bonding distance and orientation of Glu69 with respect to coordinated solvent are consistent with Glu69's *B*-factors, which resemble those of the ligands, Fe and coordinated solvent, more than those of the rest of the protein (Table 3). Thus, Q69E-FeSOD retains both the WT structure and an H-bond network like WT-Fe^{2+}SOD's, apart from the identity of the atom that distinguishes Gln from Glu. Although we have no information as to the polarity of the H-bond with coordinated solvent (and that with Tyr34), we note that all the H-bond distances in the network are

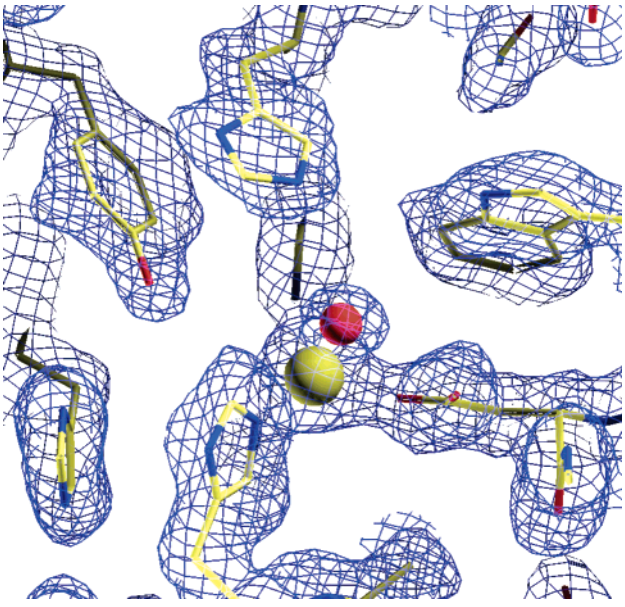

FIGURE 3: Electron density for the Q69H-FeSOD active site, viewed from the direction of ligand His160, which is therefore between the reader and the page, and not visible. $|2F_o - F_c|$ density is shown contoured at 1.5 times the rms deviation of the map.

[4] The word "atoms" is understood to mean non-hydrogen atoms, as hydrogens could not be detected in our crystal structures.

similar or slightly shorter than those of the WT active site. Although none of these differences is individually significant, considering the overall rmsd between structures, the consistency of the effect suggests more favorable H-bonding in the network in Q69E-FeSOD.[5]

In this connection, it is interesting to note that the distance between coordinated solvent and its H-bonding partner Asp156 is much longer in Q69E-FeSOD than in WT- or Q69H-FeSOD. In Q69H- and WT-FeSOD, the distances suggest that the H-bond between Asp156 and coordinated solvent is stronger than that between coordinated solvent and residue 69. However, this relationship is reversed in Q69E-FeSOD, suggesting that Glu69 effectively competes against Asp156 in its H-bonding and is thus an H-bond acceptor.

We note that a water molecule that is consistently observed in the substrate access channel of the WT-Fe^{2+}SOD structure (*13*) is also observed in our mutant structures, however at a slightly different position closer to Tyr34 (e.g., Figure 1). The difference is most pronounced in the (better-defined) Q69E-FeSOD structure and is reproduced either by allowing CNS to pick water positions or by doing so by hand. The differences between our channel waters' positions and the position obtained by Lah may reflect different data collection conditions including the lower temperature used here (115 vs 277 K) and the somewhat higher pH (*13*). However, the distances between the channel solvent molecule and His30 do not change as much as the distances between the channel solvent and Tyr34, suggesting that the latter is more likely the basis for the channel solvent's altered position in our mutants (Table 4). The similar distances obtained for the oxidized and reduced WT structures argue against an important dependence on the Fe oxidation state or protonation state of coordinated solvent. However, the two mutants' better interaction with the channel solvent may be related to their E_ms.

Redox Titrations and Equilibrations. Whereas WT-FeSOD was fully oxidized as isolated, Q69H-FeSOD was only partially ($\approx^2/_3$) oxidized, and Q69E-FeSOD was fully reduced. Thus, it was immediately evident that the E_m of Q69E-FeSOD must be very high and that of Q69H-FeSOD, intermediate. To explore the possibility that the differences in redox tuning could explain the inactivity of Q69E-FeSOD, we performed redox titrations and single-point equilibrations.

Redox titrations of Fe-SOD are notoriously difficult, as the active site Fe equilibrates very slowly (if at all) with most redox mediators (*1*, *42*, *43*), perhaps because the active site is normally accessible only to very small anions. As many of the mediators in the E_m range of interest are not stable in water for the many hours needed to complete a titration, we were not able to demonstrate reversibility. Nonetheless, our data adhere well to the Nernst equation, and the large difference between the titrations of WT- and Q69H-FeSOD indicates that the E_m of Q69H-FeSOD is $\approx$240 mV higher than that of WT-FeSOD, here measured to be 20 and 27 mV in two separate titrations (Figure 4).[6]

Q69E-Fe^{2+}SOD could not be oxidized by 1,2-naphthoquinone-4-sulfonate (E° = 628 mV, Table 5) but could be oxidized by K_2IrCl_6 (E° = 1050 mV), indicating that the reduction potential of Q69E-FeSOD is between 690 and 990 mV. Thus the reduction potential of Q69E-FeSOD appears to be at least 660 mV higher than that of WT-FeSOD.

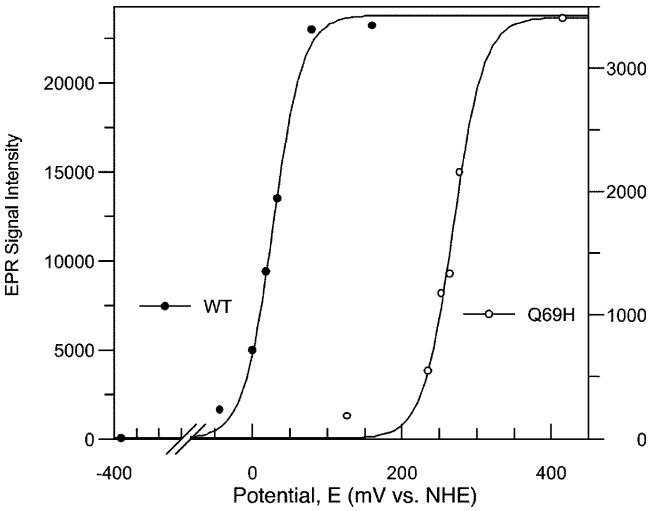

FIGURE 4: Comparison of mediated redox titrations of WT- and Q69H-FeSOD. Titrations were performed at 10 and 4 °C, respectively, as per the Materials and Methods section. Fits of the Nerst equation (2) to the data are shown, with E_m = 20 mV for WT-FeSOD and 270 mV for Q69H-FeSOD.

Table 5: Oxidants Able To Oxidize WT- and Q69E-Fe^{2+}SOD and Their Reduction Potentials

mediator/oxidant	E_m (mV) (vs NHE)	oxidation of WT-Fe^{2+}SOD	oxidation of Q69E-Fe^{2+}SOD
$KMnO_4$	1510	√	√
K_2IrCl_6	1050	√	√
$O_2^{\bullet-}$	870	√	–
1,2-naphthoquinone-4-sulfonate	628	√	–

We tried oxidizing Q69E-Fe^{2+}SOD with $O_2^{\bullet-}$, since this represents one of the two half-reactions involved in catalytic turnover. Whereas WT-Fe^{2+}SOD was rapidly reoxidized to yield the normal EPR and optical spectra of Fe^{3+}SOD, Q69E-Fe^{2+}SOD was unaffected. Thus, Q69E-Fe^{2+}SOD is not able to reduce $O_2^{\bullet-}$ on a time scale comparable to the lifetime of $O_2^{\bullet-}$ in water. This is sufficient to explain Q69E-Fe^{2+}SOD's inactivity, although other factors may contribute as well.

DISCUSSION

Q69H-FeSOD. His often takes the place of Gln in the active sites of SODs that use either Mn or Fe (Mn/FeSODs) as well as FeSODs from extremophiles (*44*, *45*). However, in these, the active site His derives from the position corresponding to Gln146 of MnSOD rather than position 69 (*35*−*38*, *46*−*48*). We refer henceforth to these SODs as His146-FeSODs. In these, His146 is argued to donate an H-bond to coordinated solvent from its Cϵ1 position (3.2 Å), while making H-bonds with Tyr34 via Nϵ2 and Trp122 via Nδ1 [Figure 5 (*36*, *37*, *46*−*48*)]. However, our His69 lacks H-bonds with Tyr34, Asn72, and Trp122 and thus has considerably more freedom. This, and the fact that our His

[5] Since the same is not observed in the Q69H-FeSOD mutant, we do not attribute it to the lower temperature used for data collection by us than by Lah et al. (*13*).

[6] The result obtained here differs from that obtained previously (*1*), and is probably more correct, as this time a cocktail of six mediators was used, vs only one mediator previously. A cocktail of mediators was used for the titration of Q69H-FeSOD as well, to improve the reliability of comparisons between the two SODs.

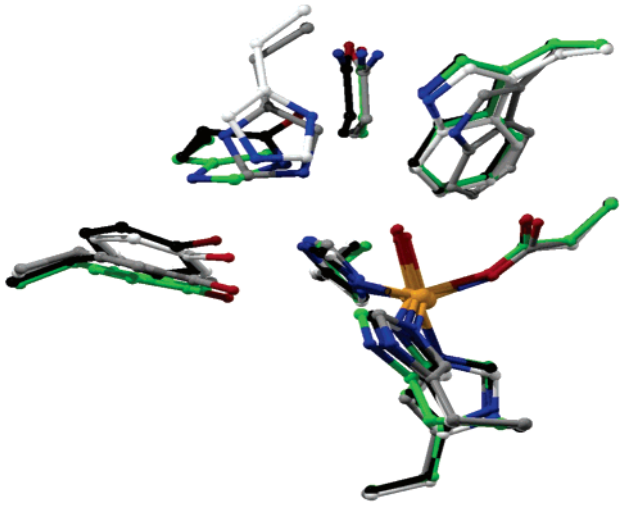

FIGURE 5: Overlay of four kinds of SOD active sites. The structure of our Q69H-FeSOD is displayed with C atoms and bonds in green, the WT-FeSOD containing a Gln at position 69 is displayed with C atoms and bonds in black, 1ISB.pdb (*13*), the structure of the mutant Q146H-MnSOD is shown with C atoms and bonds in gray, 1EN4.pdb (*46*), and the structure of *S. sulfolobus* FeSOD with a naturally occurring His at position 146 instead of Gln69 is shown with C atoms and bonds in white, 1SSS.pdb (*35*). Since *S. sulfolobus* FeSOD lacks Asn at position 72, none is shown. In all other cases all four analogous residues are shown.

derives from a completely different backbone position, can rationalize our His69's different orientation from the His' of His146-FeSODs whose crystal structures have been solved.

Q69H-FeSOD's lower than WT affinity and specificity for Fe could be related to the lack of an H-bond between residue 69 and Trp122, as this H-bond bridges the two domains of the Fe-SOD protein and its absence could allow movement of the domains relative to one another. This in turn could facilitate Fe loss, since the metal ion is bound by ligands from both domains. Like the Gln it replaces, our His69 appears to engage in a weak H-bond with coordinated solvent (3.4 Å); however, the WT Gln69 is constrained by H-bonds with Tyr34 (3.1 Å), Trp122 (3.1 Å), and Asn72 (3.3 Å), whereas His69 is not.

The identity of the His69 atom that H-bonds to coordinated solvent could be either Nϵ2 or Cϵ1; however, of these two, the more chemically likely is Nϵ2. Although the distance between our His' presumed Nϵ2 and the coordinated solvent is 3.4 Å, indicative of a weak H-bond at best, the existence of a significant interaction between Nϵ2 and coordinated solvent is demonstrated by a very large ^{15}N paramagnetic chemical shift of several hundred parts per million (Yikilmaz and Miller, unpublished results). Similarly, Edwards et al. have argued that His146 that replaces Gln146 in their Q146H-MnSOD mutant presents Nϵ2 to coordinated solvent[7] (*46*). However, the nativelike packing of His146 in Q146H-MnSOD contrasts with the *un*usual orientation of our His69 and thus suggests that the latter is the result of our His' origin at position 69, not the fact that it is taking the place of a Gln. The length of the methylene linkage to the backbone is less likely to be the cause of the different orientation, as the reverse of our mutation has been made in *Mycobacterium tuberculosis*, where the H146Q mutant reproduces the same Gln orientation as observed in *E. coli* FeSOD, even though the WT His has the orientation typical of His146-FeSODs (*49*).

Thus, we think that the His69's origin is one reason for its non-native orientation, which does not constrain it to donate an H-bond to coordinated solvent. Additional factors clearly contribute though: the *E. coli* Q146H-MnSOD has a His-to-coordinated solvent H-bond of 2.8 Å (2.0 Å resolution), whereas the six published His146-FeSODs display distances ranging from 3.10 to 3.40 Å (resolutions of 1.6−2.6 Å), for an average of 3.24 Å [$\sigma = 0.10$ Å (*35*−*38*, *47*, *48*)]. Thus, the distance displayed in *E. coli* Q146H-MnSOD is more than four standard deviations shorter than the distances observed in His146-FeSODs. The position of this residue is therefore clearly modulated by its interactions with neighbor amino acids, which are different in MnSOD and His146-FeSODs. Indeed, residues that position Trp122, which in turn affects Gln69, have been shown to modulate the strength of H-bonding between Gln69 and coordinated solvent in *Porphyromonas gingivalis* FeSOD (*25*).

H-bonding involving coordinated solvent is in turn correlated with activity and metal ion specificity. Q146H-MnSOD supports comparable Fe-based and Mn-based activity whereas His146-FeSODs are principally active with Fe (*46*). Thus, stronger H-bond donation to coordinated solvent is associated with relatively more Mn-based activity (*1*, *10*). Since stronger H-bonding to coordinated solvent will change its strength as a ligand, this could affect many elements of catalysis, including substrate binding, mode of binding, proton transfer, and the E_m (*22*, *23*, *46*, *50*, *51*). However, only the E_m has been documented here. Stronger H-bond donation to coordinated solvent in the MnSOD proteins has been proposed to disfavor acquisition of a proton by coordinated solvent in conjunction with metal ion reduction, and thus to disfavor metal ion reduction [lower the E_m (*9*, *10*)]. This would complement Mn's tendency to remain reduced and thus facilitate utilization of both oxidation states, as needed for SOD activity (*1*, *52*). Thus, it is interesting that in *P. gingivalis* FeSOD, which also supports modest but significant Mn-based activity, the distance from the Gln side chain to coordinated solvent is intermediate between those in *E. coli* FeSOD and MnSOD (*53*), and stronger H-bond donation is associated with more Mn-based activity (*25*).

Overall, Fe-based activity and the coordination geometry of the Fe site seem quite tolerant of the replacement of Gln with His, despite losses of some H-bonds in the active site and displacement of Tyr34. Mutation of Tyr34 to Phe caused loss of only 50% of WT-FeSOD activity (*39*), so our 3-fold decrease in activity could be substantially explained by loss of the H-bond between residues 69 and 34. However, the increase in E_m observed upon mutation of Gln69 to His is large, considering the conservative nature of the mutation. It seems most likely that its origin lies not in residue 69 itself but in the disruption of the H-bond network, as this would free His69 to act as an H-bond acceptor from coordinated H_2O in reduced Q69H-Fe^{2+}SOD. In contrast, Gln69 is constrained to donate an H-bond,[8] which would tend to stabilize the oxidized state instead.

[7] The distances from the Q146H-MnSOD His146 atoms to the normal H-bonding partners (Trp122 and Tyr34) nonetheless suggest that the orientation observed in His146-FeSODs is possible in this MnSOD mutant, too.

Q69E-FeSOD and a Proposed Basis for Its Inactivity. The Q69E-FeSOD active site displays only slight atomic displacements relative to the WT active site and appears to retain all of the canonical H-bonds (Figure 1). However, Q69E-FeSOD is inactive. Thus, in this mutant, the change in the chemical identity of residue 69 can be held responsible, not structural consequences of the mutation. We suggest that loss of activity can be related to Q69E-FeSOD's high E_m.

FeSOD must be able to reduce superoxide as part of turnover (eq 1b) and thus must have an E_m below that of $(O_2^{\bullet -} + 2H^+)/H_2O_2$. Indeed, WT-$Fe^{2+}$SOD could be oxidized by addition of superoxide but Q69E-FeSOD could not, indicating that Q69E-FeSOD is much less active with respect to the second half-reaction (Table 5). Q69H-FeSOD has an intermediate E_m, and it retains partial activity.

The proposed correlation can be tested qualitatively. The rate constants associated with individual steps in turnover can be related to the E_m, as shown by Han et al. (*21*). Using their eq 16 and making the provisional simplification that chemical rate constants are affected by mutation of Gln69 but the substrate on and off rates are not, consistent with retention of WT-like K_ds for substrate analogues, for Q69H-FeSOD (*9*), one can calculate the change in turnover rate expected simply due to a change in E_m. Since the mutations have stabilized the reduced state, the rate-limiting chemical step will likely be reoxidation of the metal ion, k_4. Thus

$$E_{m,mut} - E_{m,opt} = -(RT/23.06\ \text{J eV}^{-1}) \ln[(k_{4,mut}/k_{4,opt})(k_{-4,opt}/k_{-4,mut})] \quad (3)$$

where k_4 and k_{-4} are the rate constants describing the forward and backward rates of the $Fe^{2+}(H_2O)\cdot O_2^{\bullet -} + H^+ \leftrightarrow Fe^{3+}(OH^-) + H_2O_2$ reaction (*15*, *21*), with the subscripts mut and opt indicating whether the rate constant in question pertains to a mutant or WT-FeSOD. Assuming that the backward reaction accelerates by a factor similar to that by which the forward reaction decelerates (*54*) in the case of a low reorganization energy as supported by SOD's rapid turnover and very similar oxidized and reduced state crystal structures (*13*, *55*, *56*), we obtain

$$k_{4,mut} = k_{4,opt} e^{-(23.06 \text{JeV}^{-1}(E_{m,mut} - E_{m,opt})/2RT)} \quad (4)$$

Thus, a plot of the predicted percent activity retained, as a function of the shift in E_m, is provided in Figure 6. On the basis of this highly simplified model, our measured shifts in E_m should produce catalytic activities 33% and <5% of that of WT-FeSOD, for Q69H- and Q69E-FeSOD, respectively. These are in qualitative agreement with the observed relative activities of 30% and <1% observed. The predictions do not take into account additional possible bases for inactivity. Nevertheless, they indicate that the observed shifts in E_m can explain much of the decreases in activity of Q69H- and Q69E-FeSOD. Thus, within our small set of proteins, limited by the few mutations that would not produce gross structural complications, loss of activity correlates with strong elevation of E_m, in the absence of large changes in atomic positions.

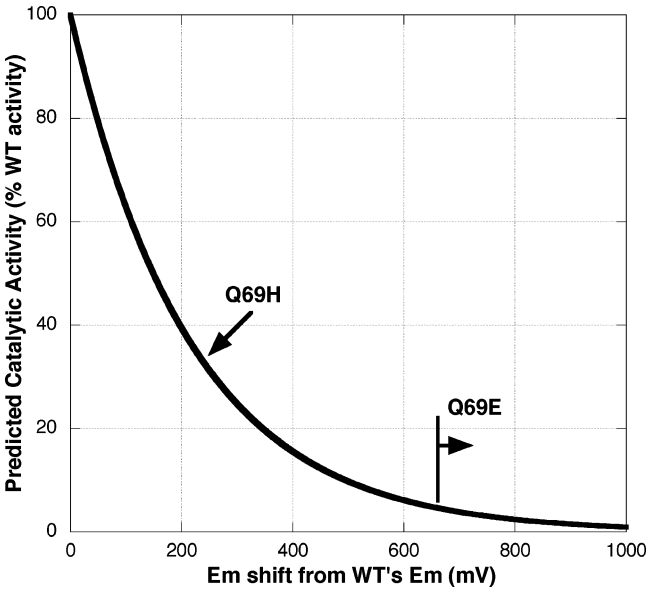

FIGURE 6: Predicted decrease in activity as a percentage of WT-FeSOD activity based on the deviation of the E_m from that of WT-FeSOD and eq 4. Q69H-FeSOD's E_m shift of 240 mV predicts retention of 33% activity and Q69E-FeSOD's shift of >660 mV predicts retention of <5% activity. The average of the limiting E_m values for Q69E-FeSOD (690 and 990 mV) yields a shift of 810 mV corresponding to <2% activity.

This example therefore provides a very clear case where the *chemical difference* between Glu69's OH and Gln's NH_2 is *more important than the positional similarities* this replacement allows. Glu will never be able to donate as many H-bonds as Gln can, and can more readily accept an H-bond. Moreover, a Glu side chain has a much higher probability of being anionic. This would make Glu^- an obligate H-bond *acceptor*, in contrast to Gln69, which is constrained to *donate* an H-bond to coordinated solvent, by the active site H-bond network. In reduced WT-FeSOD, Gln69's H-bond to coordinated H_2O appears to destabilize it relative to coordinated OH^-, in turn disfavoring the reduced state (*10*, *22*). By contrast, if the strong H-bond apparent between Glu69 and coordinated solvent corresponds to H-bond *acceptance* by Glu69, this would *stabilize* coordinated H_2O relative to coordinated OH^- and thus favor the reduced state (Figure 7). Therefore, a very subtle difference, in the polarity of the H-bond with coordinated solvent, which in turn is tightly coupled to the oxidation state of the Fe in FeSOD (*15*, *21*), could account for the different oxidation states stabilized by the two proteins.

Thus, under this proposal, the WT Gln69 is constrained to donate an H-bond, but removal of these constraints in Q69H is associated with an increase in E_m, and mutation of Gln69 to Glu transforms imposed H-bond donation from Gln69 to coordinated H_2O (*22*), into possible favorable H-bond acceptance by Glu69. Therefore, we do not claim to have engineered ≈600 mV of redox tuning into the FeSOD active site, but propose to have reversed an ≈300 mV unfavorable effect engineered by nature. Indeed, Silverman's group has shown that removal of the active site Gln146 of MnSOD results in substantial increases in protein stability (*23*, *24*). Even 300 mV corresponds to a very large energy by H-bonding standards; however, this may be dispersed over the several H-bonds that make up the active site H-bond

[8] In WT-FeSOD, Trp122 defines the polarity of the H-bond network, as it can only be an H-bond *donor*. Thus, the H-bond between Trp122 and Gln69 is assumed to engage Gln's side chain O as an H-bond acceptor, leaving Gln69's side chain amide as an H-bond donor.

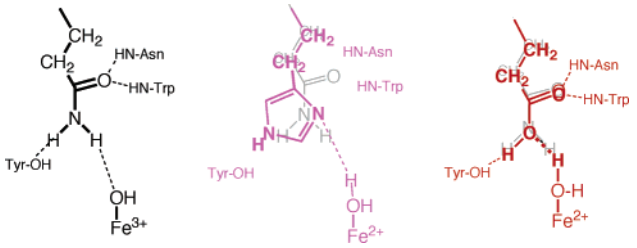

FIGURE 7: Proposed model for alterations in active site H-bonding that would be consistent with the observed increases in E_m as well as the X-ray crystal structures determined. The left panel depicts the H-bonds engaging the WT-FeSOD Gln69 to donate an H-bond to coordinated solvent, which is OH^- in the favored Fe^{3+} state. The center panel depicts the structure of Q69H-FeSOD in magenta, overlain on the structure of the WT in gray. His69 does not H-bond with nearby Trp or Asn and is therefore free to act as an H-bond acceptor in the reduced state where coordinated solvent is H_2O. The right panel depicts the structure of Q69E-FeSOD in red, overlain on the structure of the WT in gray. Glu69 is proposed to act as an H-bond acceptor to coordinated solvent, which is most likely H_2O as Fe is Fe^{2+}. This interaction is consistent with favorable H-bonds with nearby Asn, Trp, and Tyr.

network, as well as more distant interactions to which they may in turn be connected. Thus, although individual changes in H-bond distances were smaller than the rmsd between backbones, all but the H-bond to ligand Asp156 indicated more favorable H-bonding in Q69E-Fe^{2+}SOD, and the sum of the distance decreases is significant (1.7 Å, over five H-bonds).[9]

To test our hypothesis that Glu69 (and possibly His69) *accepts* an H-bond from coordinated solvent, we are seeking spectroscopic evidence for the protonation states and H-bonding activities of residue 69 in the mutants, in both oxidation states. Similarly, a higher resolution crystal structure could prove decisive, if it were able to arbitrate on the protonation state coordinated solvent and the ionization state of Glu69. These two features are crucial to the behavior of the active site and might be discernible from distances between coordinated solvent and Fe^{2+} and the C−O distances of Glu69. In the mean time, however, we argue that, in this case and likely several others too, assumptions as to the chemical nature of residues such as their protonation states, H-bonds, and the positions of labile protons in the active site should be made with considerable care. We have provided evidence here that they may have a huge effect on the oxidation state and catalytic activity of a site, which otherwise retains the WT-FeSOD structure.

ACKNOWLEDGMENT

We are grateful to Prof. Dale Webster (Illinois Institute of Technology) for the gift of toluylene blue.

SUPPORTING INFORMATION AVAILABLE

Two figures, one showing the protein monomers per unit cell in the Q69E-FeSOD structure vs the structure of Q69H-FeSOD and the other showing the ribbon structure of the Q69H-FeSOD dimer along with cocrystallized buffer molecules and crystallographic solvents. This material is available free of charge via the Internet at http://pubs.acs.org.

[9] We are not in a position to interpret this number quantitatively but simply note that it is large and may therefore help to explain the large change in E_m.

REFERENCES

1. Vance, C. K., and Miller, A.-F. (1998) A simple proposal that can explain the inactivity of metal-substituted superoxide dismutases, *J. Am. Chem. Soc. 120*, 461−467.
2. Miller, A.-F. (2004) Superoxide dismutase: An active site that saves but a protein that kills, *Curr. Opin. Chem. Biol. 8*, 162−168.
3. Rouault, T., and Klausner, R. (1997) Regulation of iron metabolism in eukaryotes, *Curr. Top. Cell. Regul. 35*, 1−19.
4. Pantopoulos, K. (2004) Iron metabolism and the IRE/IRP regulatory system: An update, *Ann. N.Y. Acad. Sci. 1012*, 1−13.
5. Wang, H., Pang, H., Bartlam, M., and Rao, Z. (2005) Crystal structure of human E1 enzyme and its complex with a substrate analog reveals the mechanism of its phosphatase/enolase activity, *J. Mol. Biol. 348*, 917−926.
6. Wierenga, R. K. (2001) The TIM barrel fold: A versatile framework for efficient enzymes, *FEBS Lett. 492*, 193−198.
7. Wise, E. L., and Rayment, I. (2004) Understanding the importance of protein structure to nature's routes for divergent evolution in TIM barrel enzymes, *Acc. Chem. Res. 37*, 149−158.
8. Park, I. Y., Eidsness, M. K., Lin, I. J., Gebel, E. B., Youn, B., Harley, J. L., Machonkin, T. E., Frederick, R. O., Markley, J. L., Smith, E. T., Ichiye, T., and Kang, C. H. (2004) Crystallographic studies of V44 mutants of *Clostridium parteurianum* rubredoxin, *Proteins: Struct., Funct., Bioinf. 57*, 618−625.
9. Yikilmaz, E. (2001) Ph.D. Thesis, pp 196, The Johns Hopkins University, Baltimore, MD.
10. Schwartz, A. L., Yikilmaz, E., Vance, C. K., Vathyam, S., Koder, R. L., Jr., and Miller, A.-F. (2000) Mutational and spectroscopic studies of the significance of the active site Gln to metal ion specificity in superoxide dismutase, *J. Inorg. Biochem. 80*, 247−256.
11. Beharry, Z. M., Eby, D. M., Coulter, E. D., Viswanathan, R., Neidle, E. L., Phillips, R. S., and Kurtz, D. M. (2003) Histidine ligand protonation and redox potential in the Rieske dioxygenases: Role of a conserved aspartate in anthranilate 1,2-dioxygenase, *Biochemistry 42*, 13625−13636.
12. Hirst, J., Duff, J. L. C., Jameson, G. N. L., Kemper, M. A., Burgess, B. K., and Armstrong, F. A. (1998) Kinetics and mechanism of redox-coupled, long-range proton transfer in an iron−sulfur protein. Investigation by fast-scan protein-film voltammetry, *J. Am. Chem. Soc. 120*, 7085−7094.
13. Lah, M. S., Dixon, M. M., Pattridge, K. A., Stallings, W. C., Fee, J. A., and Ludwig, M. L. (1995) Structure−function in *E. coli* iron superoxide dismutase: Comparisons with the manganese enzyme from *T. thermophilus*, *Biochemistry 34*, 1646−1660.
14. Miller, A.-F., Padmakumar, K., Sorkin, D. L., Karapetian, A., and Vance, C. K. (2003) Proton-coupled electron transfer in Fe−superoxide dismutase and Mn−superoxide dismutase, *J. Inorg. Biochem. 93*, 71−83.
15. Bull, C., and Fee, J. A. (1985) Steady-state kinetic studies of superoxide dismutases: Properties of the iron containing protein from *Escherichia coli*, *J. Am. Chem. Soc. 107*, 3295−3304.
16. Whittaker, J. W., and Solomon, E. I. (1988) Spectroscopic studies on ferrous non-heme iron active sites: Magnetic circular dichroism of mononuclear fe sites in superoxide dismutase and lipoxygenase, *J. Am. Chem. Soc. 110*, 5329−5339.
17. Sorkin, D. L., and Miller, A.-F. (1997) Observation of a long-predicted active site p*K* in Fe−superoxide dismutase from *E. coli*, *Biochemistry 36*, 4916−4924.
18. Jackson, T. A., Xie, J., Yikilmaz, E., Miller, A.-F., and Brunold, T. C. (2002) Spectroscopic and computational studies on iron and manganese superoxide dismutases: Nature of the chemical events associated with active site p*Ks*, *J. Am. Chem. Soc. 124*, 10833−10845.
19. Miller, A.-F., Sorkin, D. L., and Padmakumar, K. (2005) Anion-binding properties of reduced and oxidized iron-containing superoxide dismutase reveal no requirement for tyrosine 34, *Biochemistry 44*, 5969−5981.
20. Stallings, W. C., Metzger, A. L., Pattridge, K. A., Fee, J. A., and Ludwig, M. L. (1991) Structure−function relationships in iron and manganese superoxide dismutases, *Free Radical Res. Commun. 12−13*, 259−268.
21. Han, W. G., Lovell, T., and Noodleman, L. (2002) Coupled redox potentials in manganese and iron superoxide dismutases from reaction kinetics and density functional/electrostatics calculations, *Inorg. Chem. 41*, 205−218.

22. Yikilmaz, E., Xie, J., Miller, A.-F., and Brunold, T. C. (2002) Hydrogen-bond-mediated tuning of the redox potential of the nonheme Fe site of superoxide dismutase, *J. Am. Chem. Soc. 124*, 3482−3483.
23. Hsieh, H., Guan, Y., Tu, C., Bratt, P. J., Angerhofer, A., Lepock, J. R., Hickey, M. J., Tainer, J. A., Nick, H. S., and Silverman, D. N. (1998) Probing the active site of human manganese superoxide dismutase: The role of glutamine 143, *Biochemistry 37*, 4731−4739.
24. Lévêque, V. J.-P., Stroupe, M. E., Lepock, J. R., Cabelli, D. E., Tainer, J. A., Nick, H. S., and Silverman, D. N. (2000) Multiple replacements of glutamine 143 in human manganese superoxide dismutase: Effects on structure, stability and catalysis, *Biochemistry 39*, 7131−7137.
25. Yamakura, F., Sugio, S., Hiraoka, B. Y., Ohmori, D., and Yokota, T. (2003) Pronounced conversion of the metal-specific activity of superoxide dismutase from *Porphyromonas gingivalis* by the mutation of a single amino acid (Gly155Thr) located apart from the active site, *Biochemistry 42*, 10790−10799.
26. Hiraoka, B. Y., Yamakura, F., Sugio, S., and Nakayama, K. (2000) A change of the metal-specific activity of a cambialistic superoxide dismutase from *Porphyromonas gingivalis* by a double mutation of Gln-70 to Gly and Ala-142 to Gln, *Biochem. J. 345*, 345−350.
27. Schopfer, L. M., Ludwig, M. L., and Massey, V. (1991) A working proposal for the role of the apoprotein in determining the redox potential of the flavin in flavoproteins: correlations between potentials and flavin p*K*s, in *Flavins and Flavoproteins 1990* (Zanetti, G., Ed.) pp 399−404, Walter de Güyter, Berlin.
28. Barik, S. (1996) Mutagenesis and gene fusion by megaprimer PCR, *Methods Mol. Biol. 67*, 173−182.
29. Slykhouse, T. O., and Fee, J. A. (1976) Physical and chemical studies on bacterial superoxide dismutases, *J. Biol. Chem. 251*, 5472−5477.
30. McCord, J. M., and Fridovich, I. (1969) Superoxide dismutase: An enzymic function for erythrocuprein (hemocuprein), *J. Biol. Chem. 244*, 6049−6055.
31. Rodgers, D. W. (1997) *Methods Enzymol. 276*, 183−203.
32. Otwinowski, Z., and Minor, W. (1997) *Methods Enzymol. 276*, 307−326.
33. Brünger, A. T., Adams, P. D., Clore, G. M., DeLano, W. L., Gros, P., Grosse-Kunstleve, R. W., Jiang, J. S., Kuszewski, J., Nilges, M., Pannu, N. S., Read, R. J., Rice, L. M., Simonson, T., and Warren, G. L. (1998) Crystallography & NMR system: A new software suite for macromolecular structure determination, *Acta Crystallogr., Sect. D 54*, 905−921.
34. Jones, A. T., Zou, J. Y., Cowan, S. W., and Kjeldgaard, M. (1991) *Acta Crystallogr., Sect. A 47*, 110−119.
35. Ursby, T., Adinolfi, B. S., Al-Karadaghi, S., De Vendittis, E., and Bocchini, V. (1999) Iron superoxide dismutase from the archeaon *Sulfolobus solfataricus*, analysis of structure and thermostability, *J. Mol. Biol. 286*, 189−205.
36. Cooper, J. B., McIntyre, K., Badasso, M. O., Wood, S. P., Zhang, Y., Garbe, T. R., and Young, D. (1995) X-ray structure analysis of the iron-dependent superoxide dismutase from *Mycobacterium tuberculosis* at 2.0 ångstroms resolution reveals novel dimer-dimer interactions, *J. Mol. Biol. 246*, 531−544.
37. Knapp, S., Kardinahl, S., Hellgren, N., Tibbelin, G., Schäfer, G., and Ladenstein, R. (1998) Refined crystal structure of a superoxide dismutase from the hyperthermophilic archeon *Sulfolobus acidocaldaricus* at 2.2 Å resolution, *J. Mol. Biol. 285*, 689−702.
38. Schmidt, M., Meier, B., and Parak, F. (1996) X-ray structure of the cambialistic superoxide dismutase from *Propionibacterium shermanii* active with Fe or Mn, *J. Bioinorg. Chem. 1*, 532−541.
39. Sorkin, D. L., Duong, D. K., and Miller, A.-F. (1997) Mutation of tyrosine 34 to phenylalanine eliminates the active site p*K* of reduced Fe-SOD, *Biochemistry 36*, 8202−8208.
40. Whittaker, M. M., and Whittaker, J. W. (1997) Mutagenesis of a proton linkage pathway in *Escherichia coli* manganese superoxide dismutase, *Biochemistry 36*, 8923−8931.
41. Guan, Y., Hickey, M. J., Borgstahl, G. E. O., Hallewell, R. A., Lepock, J. R., O'Connor, D., Hsieh, Y., Nick, H. S., Silverman, D. N., and Tainer, J. A. (1998) Crystal structure of Y34F mutant human mitochondrial manganese superoxide dismutase and the functional role of tyrosine 34, *Biochemistry 37*, 4722−4730.
42. Verhagen, M. F. J. M., Meussen, E. T. M., and Hagen, W. R. (1995) On the reduction potentials of Fe and Cu-Zn containing superoxide dismutases, *Biochim. Biophys. Acta 1244*, 99−103.
43. Lévêque, V. J.-P., Vance, C. K., Nick, H. S., and Silverman, D. N. (2001) Redox properties of human manganese superoxide dismutase and active-site mutants, *Biochemistry 40*, 10586−10591.
44. Wintjens, R., Noël, C., May, A. C. W., Gerbod, D., Dufernez, F., Capron, M., Viscogliosi, E., and Rooman, M. (2004) Specificity and phenetic relationships of iron- and manganese-containing superoxide dismutases on the basis of structure and sequence, *J. Biol. Chem. 279*, 9248−9254.
45. Smith, M. W., and Doolittle, R. F. (1992) A comparison of evolutionary rates of the two major kinds of superoxide dismutase, *J. Mol. Evol. 34*, 175−184.
46. Edwards, R. A., Whittaker, M. M., Whittaker, J. W., Baker, E. N., and Jameson, G. B. (2001) Outer sphere mutations perturb metal reactivity in manganese superoxide dismutase, *Biochemistry 40*, 15−27.
47. Lim, J.-H., Yu, Y. G., Han, Y. S., Cho, S., Ahn, B.-Y., Kim, S.-H., and Cho, Y. (1997) The crystal structure of an Fe-superoxide dismutase from the hyperthermophile *Aquifex pyrophilus* at 1.9 Å resolution: Structural basis for thermostability, *J. Mol. Biol. 270*, 259−274.
48. Adams, J. J., Anderson, B. F., Renault, J. P., Verchere-Beaur, C., Morgenstern-Badarau, I., and Jameson, G. B. (2002) Structure and properties of the atypical irion superoxide dismutase from *Methanobacterium thermoautotrophicum*, RCSB 1MA1.
49. Bunting, K., Cooper, J. B., Badasso, M. O., Tickle, I. J., Newton, M., Wood, S. P., Zhang, Y., and Young, D. (1998) Engineering a change in metal-ion specificity on the iron-dependent superoxide dismutase from *Mycobacterium tuberculosis* X-ray structure analysis of site-directed mutants, *Eur. J. Biochem. 251*, 795−803.
50. Jackson, T. A., Yikilmaz, E., Miller, A.-F., and Brunold, T. C. (2003) Spectroscopic and computational study of a non-heme iron {Fe−NO}7 system: Exploring the geometric and electronic structures of the nitrosyl adduct of iron superoxide dismutase, *J. Am. Chem. Soc. 125*, 8348−8363.
51. Xie, J., Yikilmaz, E., Miller, A.-F., and Brunold, T. C. (2002) Second-sphere contributions to substrate analog binding in iron(III) superoxide dismutase, *J. Am. Chem. Soc. 124*, 3769−3774.
52. Vance, C. K., and Miller, A.-F. (2001) Novel insights into the basis for *E. coli* SOD's metal ion specificity, from Mn-substituted Fe-SOD and its very high E_m, *Biochemistry 40*, 13079−13087.
53. Sugio, S., Hiraoka, B. Y., and Yamakura, F. (2000) Crystal structure of cambialistic superoxide dismutase from *Porphyromonas gingivalis*, *Eur. J. Biochem. 267*, 3487−3495.
54. Marcus, R. A., and Sutin, N. (1985) Electron transfers in chemistry and biology, *Biochim. Biophys. Acta 811*, 265−322.
55. Fee, J. A., McClune, G. J., O'Neill, P., and Fielden, E. M. (1981) Saturation behavior of superoxide dismutation catalyzed by the iron containing superoxide dismutase of *E. coli*, *Biochem. Biophys. Res. Commun. 100*, 377−384.
56. Bull, C., Niederhoffer, E. C., Yoshida, T., and Fee, J. A. (1991) Kinetic studies of superoxide dismutases: Properties of the manganese-containing protein from *Thermus thermophilus*, *J. Am. Chem. Soc. 113*, 4069−4076.
57. Miller, A.-F. (2001) Fe-superoxide dismutase, in *Handbook of Metalloproteins* (Wieghardt, K., Huber, R., Poulos, T., and Messerschmidt, A., Eds.) Vol. 1, pp 668−682, Wiley and Sons, New York.

BI051495D